

Phase-dependence of sorption-induced mass streaming in an acoustic field

Cite as: Appl. Phys. Lett. **115**, 033703 (2019); <https://doi.org/10.1063/1.5110601>

Submitted: 19 May 2019 . Accepted: 26 June 2019 . Published Online: 18 July 2019

Yuval Blayer, Nimrod Elkayam, and Guy Z. Ramon 



View Online



Export Citation



CrossMark



Sensors, Controllers, Monitors
from the world leader in cryogenic thermometry



Phase-dependence of sorption-induced mass streaming in an acoustic field

Cite as: Appl. Phys. Lett. **115**, 033703 (2019); doi: [10.1063/1.5110601](https://doi.org/10.1063/1.5110601)

Submitted: 19 May 2019 · Accepted: 26 June 2019 ·

Published Online: 18 July 2019



View Online



Export Citation



CrossMark

Yuval Blayer,^{1,3,a)} Nimrod Elkayam,^{2,3,a)} and Guy Z. Ramon^{2,3,b)} 

AFFILIATIONS

¹The Applied Mathematics Interdisciplinary Graduate Program, Technion - Israel Institute of Technology, Haifa 32000, Israel

²The Nancy and Stephen Grand Technion Energy Program, Technion - Israel Institute of Technology, Haifa 32000, Israel

³Department of Civil and Environmental Engineering, Technion - Israel Institute of Technology, Haifa 32000, Israel

^{a)}Contributions: Y. Blayer and N. Elkayam contributed equally to this work.

^{b)}ramong@technion.ac.il

ABSTRACT

A nonzero time-averaged mass flux is generated in oscillating flows due to phase-lags between the fluctuating velocity field and the diffusive transport. Herein, we demonstrate how, in addition, the acoustic phasing of a sound wave—the phase difference between pressure and velocity oscillations—interacts with material properties and geometry to affect the preferential transport of a “reactive” species undergoing reversible sorption. Experimental results illustrate how phasing affects the induced mass flux, its dependence on the diffusive and oscillation time-scales, and how they compare well with model calculations. The model is used to reveal the underlying mechanisms that generate the concentration gradient, vs those that dissipate it. This insight can assist the future development and design of acoustic gas separation processes.

Published under license by AIP Publishing. <https://doi.org/10.1063/1.5110601>

Nonzero, time-averaged fluxes of scalars, e.g., heat and mass, can be generated in oscillating velocity fields. In the case of mass transport within a mixture, a preferential flux of a component may be created, leading to separation. The use of an oscillating, incompressible velocity field for separation has been demonstrated in several configurations. Notably, these fluxes are proportional to and directed down a concentration gradient imposed on the system^{1–6} (as in Taylor-Aris dispersion). In contrast, it has been shown that when an acoustic field is applied, i.e., compression and expansion are also present, this gradient may be created by the time-averaged flux (termed “streaming” in analogy with the non-linear bulk motion generated in fluctuating velocity fields⁷). The mechanism driving this type of mass streaming can originate from thermal-diffusion^{8,9} or, as has been recently shown, from mass exchange with a boundary, e.g., through reversible adsorption.¹⁰ In all these cases, streaming is achieved through temporal “storage” of a component, either within a lower velocity region (near a solid boundary) or within a sorbent layer coating the boundary. The streaming flux is generated by phase lags between the axial motion and lateral fluxes during an oscillation cycle. In the acoustic case, phase lags are also created by changes in local equilibrium due to compression/expansion—these can drive heat and mass transfer from the fluid to the solid boundary.^{10,11}

Evidently, the phasing between pressure and velocity and the way they interact with the characteristic time-scales of the lateral transport

can conspire to dictate the resultant streaming flux. Herein, we generalize the framework, set out by Weltsch *et al.*¹⁰ for the particular case of a standing wave (SW) acoustic phasing, so as to consider the full range of acoustic phases and reveal the interplay between the underlying mechanisms.

In order to experimentally control the acoustic phasing of the generated field, a device was constructed, comprising two opposing acoustic drivers connected by a short tube [see Fig. 1(a)]. A 10 cm-long, steel honeycomb “stack,” dip-coated with Zeolite 13X adsorbent, is placed in the tube, slightly closer to the right driver. Three stacks were used, with average channel dimensions of $h \approx 0.25, 0.5,$ and 1 mm. The fluid mixture used was ambient air, in which water vapor represents the “reactive” fluid that interacts with the solid boundary. The mass streaming is detected by monitoring the humidity at both ends of the stack, converted, at a given temperature (measured by the humidity sensor) and absolute pressure, to the molar fraction C . The difference in molar fraction along the stack, ΔC , is the result of the mass streaming generated by the applied acoustic field. Initial experiments used heat exchangers (similar to those reported in Ref. 10), so as to maintain isothermal conditions; however, these were found to be unnecessary in the employed range of pressure amplitudes, and the temperature difference was generally below 2°C (for these measurements and further details of the experiments, please refer to the [supplementary material](#)).

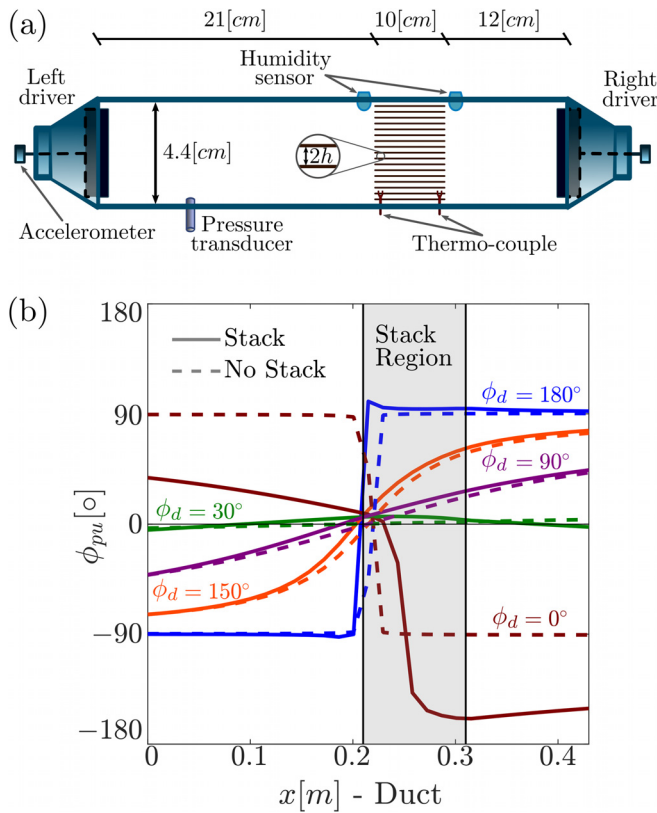


FIG. 1. (a) Schematic drawing of the experimental apparatus. Linear motor-driven pistons are positioned at either ends of a tube, enabling independent control of velocity amplitude, frequency, and phase. An adsorbent-coated metal stack is placed within the tube, with humidity and temperature sensors at both ends. Pressure and acceleration are measured on the left driver. (b) Calculated acoustic phasing ϕ_{pu} (representing the phase angle between the pressure and velocity) along the tube, for different values of ϕ_d (representing the phase angle between the motion of the left and right drivers). Dashed and solid lines represent cases with and without the stack, respectively.

In what follows, we define the acoustic phase, $\phi_{pu} \in [-180^\circ, 180^\circ]$, as the phase difference between the oscillations of pressure and velocity at a point. This phase represents a traveling wave (TW) at values of $(0^\circ, \pm 180^\circ)$, where the crests of pressure and velocity are simultaneous, and a standing wave (SW) at values of $(\pm 90^\circ)$, where the pressure extremes occur at zero velocity. Operating both drivers at the same amplitude and frequency creates an acoustic field, which can be expressed as a function of ϕ_d , the phase lag between the drivers. The “ideal” velocity field may then be written as¹²

$$u_1 = \alpha e^{i(\omega t - kx)} + \beta e^{i(\omega t + kx)}, \quad (1)$$

in which

$$\alpha = -U_0 \left[\frac{e^{ikL} - e^{i\phi_d}}{e^{-ikL} - e^{ikL}} \right]; \quad \beta = U_0 \left[\frac{e^{-ikL} - e^{i\phi_d}}{e^{-ikL} - e^{ikL}} \right], \quad (2)$$

where L is the length of the tube, $k = \omega/a$ is the wave-number, and a is the speed of sound. For $\phi_d = \pm kL$, either α or β , the coefficients of the left- or right-moving TW reach zero, and a pure TW is created.

A pure SW appears when $\phi_d = 0, \pm 180^\circ$, with a pressure node (zero pressure, maximum velocity) or pressure antinode (maximal pressure, zero velocity) at the midpoint of the duct. The acoustic intensity scales as $I \sim \sin \phi_d$ (zero for each of the SW modes), which is maximized when $\phi_d = \pm 90^\circ$. Figure 1(b) shows the calculated acoustic phasing along the tube for different values of ϕ_d with and without the stack present (for details of these calculations, please refer to the [supplementary material](#)). We note that for most values of ϕ_d , the deviation between the two cases is rather small, indicating that the short stack at the given location inside the long wave presents a small interference. For example, at $\phi_d = 30^\circ \approx kL$, a consistently small ϕ_{pu} implies a small deviation from the ideal (TW) field. However, at $\phi_d = 0^\circ$, ϕ_{pu} changes rapidly within the stack and can no longer be considered a SW field. At $\phi_d = 90^\circ$, a low ϕ_{pu} within the stack indicates a dominant TW component and with double the intensity of $\phi_d = 30^\circ$, it can be considered to be the dominant TW mode. On the other hand, $\phi_d = 180^\circ$ maintains an approximately ideal SW field, even with the stack present.

The main result of the experiments is the measurement of the concentration difference developing when a given acoustic field is applied. An illustration of the concentration distribution within the tube is shown in Fig. 2(a), for various acoustic fields (represented by ϕ_d). The experimental measurements are summarized in Fig. 2(b), showing the concentration difference across the stack, scaled against the initial concentration, $\widehat{\Delta C} = \Delta C/C_0$. The measured points were taken following 30 min of steady operation (the time required to reach equilibrium) at different values of ϕ_d and $\tau_D \equiv h(\omega/D)^{1/2}$, which represents the ratio of the diffusion time scale to the oscillation time scale, where D is the diffusivity of the vapor. Also shown are calculations based on the numerical solution of the acoustic field and the time-averaged concentration field at equilibrium (i.e., at long times when the overall mass flux is zero),¹⁰ which, in the scaled form, is given by

$$\left. \frac{dC_m}{dx} \right|_{lim} = - \frac{C_m |u_1| \left(\frac{|p_1|}{p_m} \right) M[\phi_{pu}, \tau_D, Sc]}{|u_1|^2 G[\tau_D, Sc] + 2Pe^{-1}}, \quad (3)$$

where $|u_1|$ is the velocity amplitude, scaled by the speed of sound a , $|p_1|$ and p_m denote the pressure amplitudes at point x and the mean pressure, respectively, scaled by ρa^2 , and $Pe = a \lambda/D$ is a “Péclet” number accounting for the contribution of longitudinal diffusion, in which λ is the acoustic wavelength. The numerator represents the acoustic flux that creates the gradient, in which $M[\phi_{pu}, \tau_D, Sc]$ determines how ϕ_{pu} and the geometry affect the mass flux, where $Sc = \nu/D$ is the Schmidt number. In contrast, the denominator contains the “destructive” flux (in the sense that it transports mass down the gradient), consisting of molecular diffusion and Taylor-Aris dispersion, which is proportional to $|u_1|^2$ and $G[\tau_D, Sc]$ embodying the effect of geometry, Sc , and the frequency (see further details of the derivation in the [supplementary material](#)).

The experimental measurements of the concentration difference across the stack at equilibrium, $\widehat{\Delta C}$, are shown in Fig. 2(b) as a function of ϕ_d , as are model calculations. Model and experiment demonstrate a fair agreement, but there is some deviation due to several possible reasons. First, the small temperature differences developed in our system are not accounted for in the model. These are estimated, at most, to produce a 10%–15% deviation under saturated conditions. In

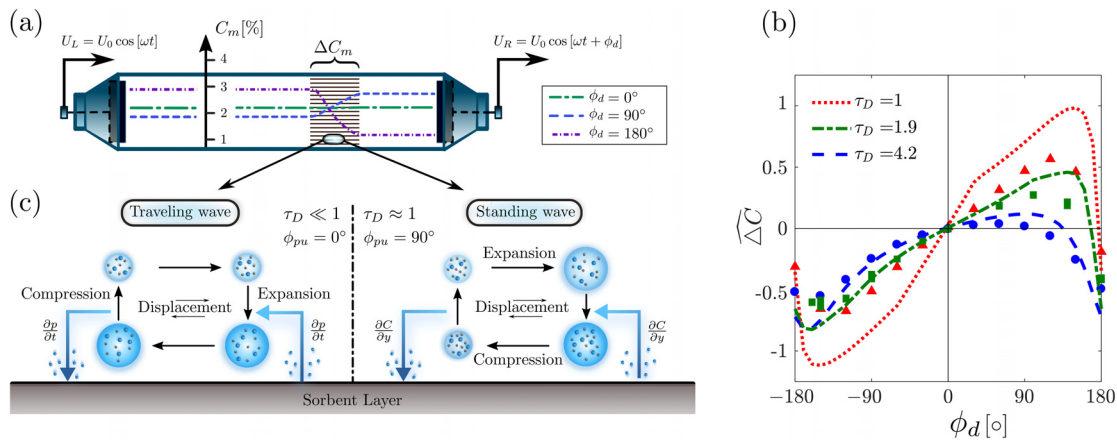


FIG. 2. (a) Illustration of the concentration field within the system under representative acoustic fields, defined by the phase difference between the drivers, ϕ_d . The concentrations were calculated for $\tau_D \equiv h(\omega/D)^{1/2} = 1.9$. (b) Calculated (lines) and measured (points) concentration difference across the stack at equilibrium, $\Delta \widehat{C} \approx \Delta C/C_0$, scaled by the initial concentration, as a function of ϕ_d . Here, $U_0 \approx 0.7 \text{ m s}^{-1}$, $\omega \approx 378 \text{ s}^{-1}$, and $D \approx 2.8 \times 10^{-5} \text{ m}^2 \text{ s}^{-1}$. (c) The simplified mechanism: sorption(desorption) occurs during compression(expansion), and combined with the oscillatory motion, generates the mass streaming. In a standing wave, displacement and mass exchange with the boundary occur simultaneously, while in a traveling wave, mass exchange to/from the boundary occurs primarily at the extremes of the displacement.

the interest of simplicity, we opt to leave the full account of temperature-concentration coupling to future work. Furthermore, the exact location of the moving boundaries is not captured in the model, creating a small uncertainty in the position of the stack within the acoustic field. Finally, the possibility of competitive adsorption between various components is neglected (only vapor is assumed to be reactive). These all appear to be reasonable assumptions, but obviously affect, to a relatively small extent, the accuracy of the model predictions. Examining the full range of phases, ϕ_d , we note that for all cases, $\Delta \widehat{C}$ has a negative minimum and a positive maximum, representing the phasing that maximizes the mass streaming in one direction or the other (when $\Delta \widehat{C} = 0$, these cancel out entirely). These singular points turn out to be at $90^\circ < |\phi_d| < 180^\circ$ (recall that for $\phi_d = 180^\circ$, the acoustic field is a SW, while for $\phi_d = 90^\circ$, it is much closer to a TW). On the rest of the spectrum ($|\phi_d| < 90^\circ$), the acoustic field apparently drives a weaker streaming, possibly due to the lower pressure amplitude, which has a minimum value at $\phi_d = 0^\circ$. In addition, $\Delta \widehat{C}$ is increased as τ_D decreases, for nearly all phases, which can be attributed to the larger specific surface area of the more confined geometry.

Furthermore, we notice a difference in the shape of the curves with τ_D . For $\tau_D = 1$, the profile is almost antisymmetric with respect to $\phi_d = 0^\circ$, i.e., setting ϕ_d to a positive or negative value would not affect the magnitude of the streaming flux, but will determine its direction. Meanwhile, for $\tau_D = 4.2$, the positive gradient nearly vanishes, and the negative minimum tends toward $\phi_d = -180^\circ$ (SW phasing). This observation reflects the actual effect of acoustic phasing on mass streaming, which is dominated by TW phasing in confined geometries and by SW phasing for larger channel dimensions. This insight relies not only on the higher streaming observed for SW phasing at larger τ_D , but also on the trend in the shape of the profiles. A traveling wave has a clear direction, which dictates the mass transport, while a standing wave will pump mass toward the pressure antinode. Bidirectional mass streaming, at similar magnitudes, was observed only for the smallest τ_D , where TW phasing is favored.

The conceptual mechanism behind the observed phase-dependence of the induced concentration gradient is schematically depicted in Fig. 2(c), following idealized 4 stages of the acoustic cycle, for traveling and standing wave phasing within channels spaced at a distance that is comparable to, or much smaller than, the diffusive length accessible during an oscillation period, i.e., $h \ll (D/\omega)^{1/2}$ or $h \sim (D/\omega)^{1/2}$, respectively. In general, compression and expansion drive mass exchange with the boundary due to deviation of the equilibrium at high and low pressures, respectively. However, for the standing wave, displacement is in phase with compression/expansion, such that mass exchange between the boundary and the gas mixture occurs during motion, only if a gradient is established between the boundary and the bulk concentrations. For this to happen, there must be a distance over which a gradient may develop during the oscillation half-cycle, hence the need for a channel spacing on the order of the diffusive penetration depth, or equivalently, $\tau_D \sim 1$.

Meanwhile, in the traveling wave displacement and compression/expansion are out-of-phase, such that sorption/desorption occurs following the displacement, driven by the pressure change, dp_1/dt . In this case, streaming is maximized when the gas mixture is at local equilibrium with the boundary during the displacement, achieved by maintaining $\tau_D \ll 1$. Mass transfer is generated despite this local equilibrium since the composition of the mixture changes concurrently with the pressure, in accordance with the relation $C_1 = -(C_m/p_m)p_1$, representing equilibrium between the mixture and the sorbent during the oscillation (subscript “1” denotes a fluctuation).¹⁰ In this manner, no significant lateral concentration gradients are required for the mass exchange, so that the process is thermodynamically favorable due to smaller entropy generation. The increased flux created in the traveling wave may also be explained, from a Eulerian viewpoint, as due to a larger overall concentration carried by the velocity field (see [supplementary material](#) for Eulerian description of the mechanism).

The relationship between the flux, acoustic phase and the geometry is further illustrated in Fig. 3. The calculated “limiting” concentration gradient (i.e., the maximum achievable gradient, when the total

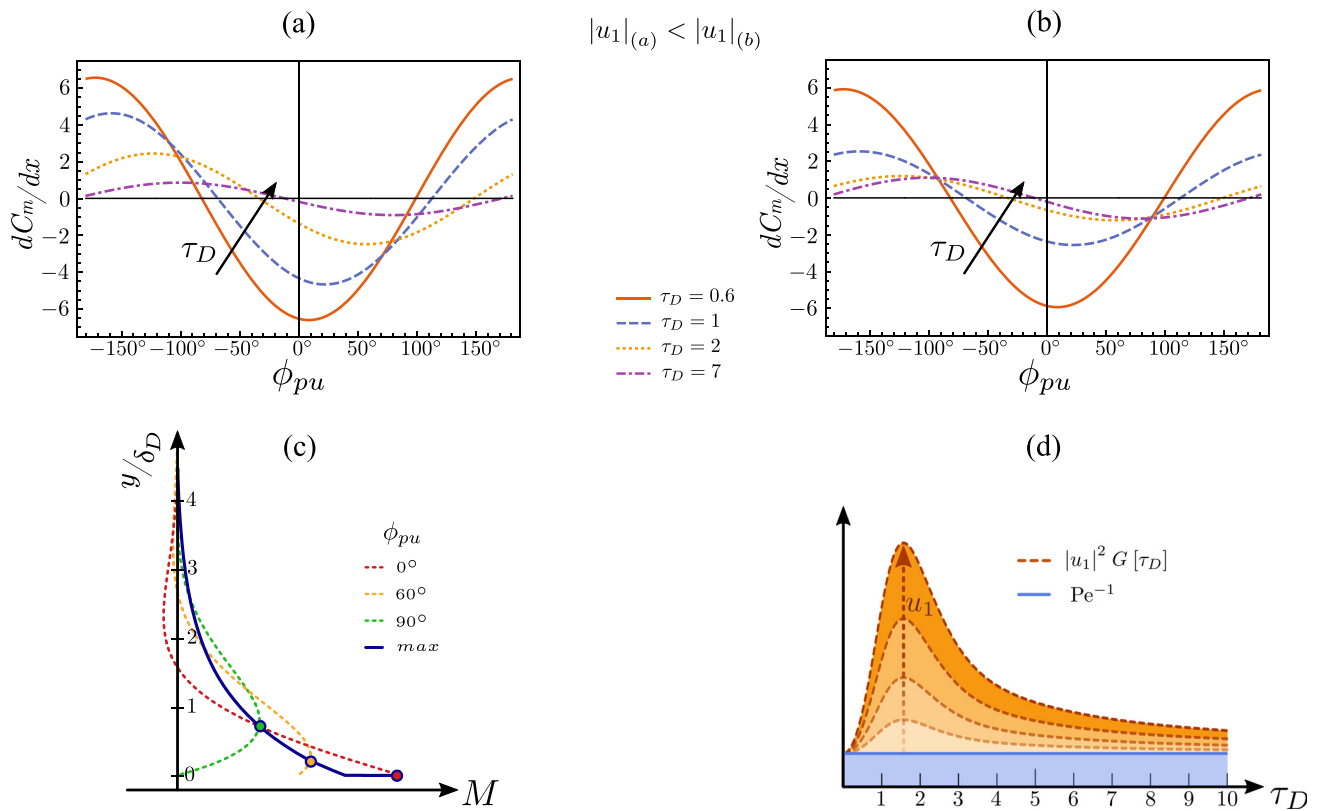


FIG. 3. Model calculations of the mass-streaming mechanisms. (a) and (b) Show the time-averaged limiting concentration gradient, as a function of the acoustic phasing, ϕ_{pu} , and for various values of $\tau_D \equiv h(\omega/D)^{1/2}$. The velocity amplitude in (a) is smaller than in (b). (c) Variation of the time-averaged mass flux as a function of the distance from the sorbing boundary (at short times, before the gradient is established), as a function of ϕ_{pu} . The continuous blue line connects the points at which the maximum flux is created at different phases. (d) The relative magnitude of the destructive flux (down the concentration gradient), consisting of molecular diffusion (blue shade) and Taylor-Aris dispersion (brown shade), as a function of τ_D .

mass flux vanishes) is shown in Figs. 3(a) and 3(b), illustrating its dependence on acoustic phasing and geometry, when taking into account both the beneficial and destructive fluxes—creating and dissipating the gradient, respectively. In each plot, conditions are identical, while τ_D is varied, at two different velocity amplitudes. The magnitude of the streaming flux created with $\phi_{pu} = 0$ and $\tau_D \ll 1$ will tend to be larger than when $\phi_{pu} > 0$ and $\tau_D \sim 1$ under otherwise identical conditions. This claim is based on the fact that when $h \ll (D/\omega)^{1/2}$, the concentration profile is uniform (at a value set by the largest or lowest pressure in the cycle), and therefore the flux, being a product of concentration and velocity, is larger. This is further evident from a calculation of the acoustic flux component that pumps mass up the gradient, as a function of the distance from the sorbing boundary, which is maximized at an acoustic phase $\phi_{pu} = 0$ and occurs near the boundary, as shown in Fig. 3(c).¹³ Furthermore, the destructive flux, which is proportional to the concentration gradient, is not a function of ϕ_{pu} and includes two components as shown in Fig. 3(d). One component is due to diffusion and is manifested in a scaled form as a function of the Péclet number. The second term is due to the oscillatory Taylor-Aris dispersion and is proportional to $|u_1|^2$. Being strongly dependent on τ_D , this flux has a distinctive peak when $h \sim (D/\omega)^{1/2}$, that is, when $\tau_D \sim O(1)$, rapidly decaying for both low and high τ_D . Because of this

destructive effect at high velocity amplitudes, it is more effective to increase the drive ratio p_1/p_m in order to create a larger gradient.

In summary, we have presented experiments that demonstrate the dependence of an acoustically-driven mass flux on the phasing between pressure and velocity fluctuations. The mass flux is generated due to the mass exchanged between the gas mixture and a sorbing solid, driven by pressure oscillations that modify the local gas-solid equilibrium for a reactive component in the mixture. The nonlinear interaction of the velocity, pressure, and concentration fields results in a time-averaged flux that depends strongly on the phasing, and is shown to be maximized for near traveling-wave fields. This is captured in a theoretical model that shows a fair agreement with experiments. The underlying mechanism is most simply explained as the result of mass exchange occurring during periods of large temporal pressure changes with very little concurrent motion or, equivalently, by cross-sectional equilibration of the gas component, before it is advected by the velocity field. The presented results and framework further substantiate the capacity for mixture separation in acoustic fields, while highlighting the main attributes necessary for the future design of efficient separators—traveling wave phasing with a large pressure amplitude, small velocity amplitude, and a confined geometry.

See the [supplementary material](#) for further details on the experimental methods, temperature variation in experiments, derivation of the key equations, and a more detailed Eulerian description of the mass transfer mechanism.

This research was supported by Grant No. 216-11-024 from the Israel Ministry of Energy and Water. N.E. acknowledges the support from the Nancy and Stephen Grand Technion Energy Program (GTEP).

REFERENCES

- ¹M. Shapiro and H. Brenner, *Chem. Eng. Sci.* **41**, 1417 (1986).
- ²U. H. Kurzweg and M. J. Jaeger, *Phys. Fluids* **30**, 1023 (1987).
- ³B. S. Mazumder and S. K. Das, *J. Fluid Mech.* **239**, 523 (1992).
- ⁴C. O. Ng, *Int. J. Eng. Sci.* **38**, 1639 (2000).
- ⁵C.-O. Ng, *Proc. R. Soc. A* **462**, 481 (2006).
- ⁶G. Ramon, Y. Agnon, and C. Dosoretz, *Microfluid. Nanofluid.* **10**, 97 (2011).
- ⁷N. Riley, *Annu. Rev. Fluid Mech.* **33**, 43 (2001).
- ⁸G. W. Swift and P. S. Spoor, *J. Acoust. Soc. Am.* **106**, 1794 (1999).
- ⁹P. S. Spoor and G. W. Swift, *Phys. Rev. Lett.* **85**, 1646 (2000).
- ¹⁰O. Weltsch, A. Offner, D. Liberzon, and G. Z. Ramon, *Phys. Rev. Lett.* **118**, 244301 (2017).
- ¹¹G. W. Swift, *Thermoacoustics: A Unifying Perspective for Some Engines and Refrigerators* (Acoustical Society of America, 2003).
- ¹²L. E. Kinsler, A. R. Frey, A. B. Coppens, and J. V. Sanders, *Fundamentals of Acoustics* (Wiley, 2001).
- ¹³Note that this idealized representation is slightly skewed by the no-slip condition, but is qualitatively representative.